PCCP

RSC Publishing

PAPER

View Article Online
View Journal | View Issue



Cite this: *Phys. Chem. Chem. Phys.*, 2013, **15**, 12241

# Vibrational Stark effect spectroscopy reveals complementary electrostatic fields created by protein–protein binding at the interface of Ras and Ral

David M. Walker, Ellen C. Hayes and Lauren J. Webb*

Received 26th March 2013,
Accepted 2nd June 2013

DOI: 10.1039/c3cp51284c

www.rsc.org/pccp

Electrostatic fields at the interface of the GTPase H-Ras (Ras) docked with the Ras binding domain of the protein Ral guanine nucleoside dissociation stimulator (Ral) were measured with vibrational Stark effect (VSE) spectroscopy. Nine residues on the surface of Ras that participate in the protein–protein interface were systematically mutated to cysteine and subsequently converted to cyanocysteine in order to introduce a nitrile VSE probe into the protein–protein interface. The absorption energy of the nitrile was measured both on the surface of Ras in its monomeric state, then after incubation with the Ras binding domain of Ral to form the docked complex. Boltzmann-weighted structural snapshots of the nitrile-labeled Ras protein were generated both in monomeric and docked configurations from molecular dynamics simulations using enhanced sampling of the cyanocysteine side chain's $\chi_2$ dihedral angle. These snapshots were used to determine that on average, most of the nitrile probes were aligned along the Ras surface, parallel to the Ras–Ral interface. The average solvent-accessible surface areas (SASA) of the cyanocysteine side chain were found to be $<60$ Å$^2$ for all measured residues, and was not significantly different whether the nitrile was on the surface of the Ras monomer or immersed in the docked complex. Changes in the absorption energy of the nitrile probe at nine positions along the Ras–Ral interface were compared to results of a previous study examining this interface with Ral-based probes, and found a pattern of low electrostatic field in the core of the interface surrounded by a ring of high electrostatic field around the perimeter of the interface. These data are used to rationalize several puzzling features of the Ras–Ral interface.

## Introduction

Understanding the noncovalent mechanisms of protein–protein interactions in the complex environment of the living cell is a current problem of immense importance in biochemistry and biophysics. Nearly all known protein–protein complexes are assembled noncovalently, the result of the combination of structural complementarity and electrostatic forces.[1–3] While a growing database of experimentally determined protein–protein complexes can be found in the protein data bank, the role of electrostatic forces in determining the binding energies, rates, structures, and functions of protein–protein complexes has largely eluded experimental study. Recently our laboratory has demonstrated the effectiveness of measuring perturbations in the electrostatic environment of a protein surface and protein–protein interface using vibrational Stark effect (VSE) spectroscopy of unnatural functional groups acting as electrostatic probes.[4–6] VSE spectroscopy relates changes in the vibrational absorption energy, $\Delta\bar{\nu}_{\mathrm{obs}}$, of a harmonic oscillator to its local electrostatic field through eqn (1):[7–9]

$$\Delta E_{\mathrm{protein}} = hc\Delta\bar{\nu}_{\mathrm{obs}} = -\Delta\vec{\mu}\cdot\Delta\vec{F}_{\mathrm{protein}} \quad (1)$$

where $\Delta\vec{\mu}$ is the difference between the oscillator's ground and excited state dipole moments and is unique to the vibrational oscillator, and $\Delta\vec{F}_{\mathrm{protein}}$ is the change in electrostatic field projected onto $\Delta\vec{\mu}$ caused by a chemical or physical perturbation to the probe and compared with a known reference state. The probe molecule's vibrational absorption energy is therefore a reporter of the local electrostatic field surrounding the probe,[9] and quantifies changes in this energy from controlled perturbations, allowing the magnitude and direction of a protein's electrostatic field to be measured directly and defined *versus* some useful reference state.[10–12]

Our laboratory has investigated the role of electrostatic forces in forming stable protein–protein interactions through

*Department of Chemistry and Biochemistry, Institute for Cell and Molecular Biology, and Center for Nano- and Molecular Science and Technology, The University of Texas at Austin, 1 University Station A5300, Austin, TX 78712, USA. E-mail: lwebb@cm.utexas.edu; Fax: +1 512-471-9361*

VSE using a nitrile probe that can be systematically moved throughout the protein–protein interface by chemically labeling cysteine residues added to the protein through amino acid mutagenesis.[4,5,12,13] By comparing a nitrile's vibrational absorption energy between a monomeric protein and a docked protein–protein complex, the electrostatic perturbations that occur upon docking can be thoroughly examined. Because $\Delta\vec{\mu}$ is parallel to the bond axis of the nitrile diatomic oscillator, the chromophore is sensitive to electrostatic fields projected onto the nitrile bond.[7] In addition, $\Delta\vec{\mu}$ for a thiocyanate has been calibrated to be roughly 0.7 $cm^{-1}$ $(MV/cm)^{-1}$, meaning that every one MV $cm^{-1}$ field change will correspond to a 0.7 wavenumber shift in energy.[4,7] This means the nitrile has exceptional sensitivity to measuring differences in electrostatic fields through vibrational spectroscopy. Interpreting vibrational absorption data in terms of electrostatic fields therefore requires that the position and orientation of the probe in the biomolecule be known to a high degree of certainty, along with the range of conformational states that are sampled by the cyanocysteine side chain during a room temperature steady-state experiment. We therefore also carry out extensive molecular dynamics (MD) with enhanced sampling to generate a Boltzmann-weighted ensemble of probe orientations that is then used to interpret vibrational energies in terms of electrostatic fields experienced by the nitrile vibrational probe. These explicit water MD simulations also allow the degree of solvent accessibility to the vibrational probe to be determined, which in turn can be used to evaluate the extent to which chemical changes to the nitrile such as hydrogen bond formation play in changes to the measured vibrational absorption energy.[14,15]

The human oncoprotein $p21^{Ras}$, of which H-Ras is a member (hereafter called "Ras"), is a guanosine triphosphate (GTP)-binding protein involved in several signal transduction cascades that propagate chemical information throughout the healthy cell.[16–19] When bound to GTP, Ras is known to dock to several so-called downstream effector proteins for the propagation of signal transduction cascades for a variety of functions.[20–22] Several such downstream effectors are c-Raf-1 (hereafter "Raf") to initiate the MAP kinase cascade for cell division,[22] phosphatidylinositol 3-kinase (PI3K) to promote transcription and cytoskeletal signaling,[23,24] and Ral guanine nucleotide dissociation stimulator (RalGDS, hereafter called "Ral") to promote vesicle transport.[17,25,26] It is vital that Ras dock with the appropriate downstream effector to propagate a specific signal transduction cascade based on the needs of cell survival. Furthermore, Ras must distinguish its appropriate downstream effectors from other effector proteins that dock with many alternative GTPases.[17,20,27] While cell trafficking and localization mechanisms are responsible for some of this control and discrimination,[20,25,26] it is known that *in vitro*, Ras binds to these downstream effectors with different rates (dissociation constants of ~18 nM,[16,27] ~1 μM,[4,27] and ~3.2 nM[28,29] for Raf, Ral, and PI3K, respectively). Ras therefore must have a noncovalent mechanism to identify and dock with an appropriate downstream effector to promote the function necessary for the cell, even in the absence of cellular regulation.[20–27] This noncovalent mechanism could be both structural and electrostatic in origin; however several crystal structures of these downstream effectors demonstrate their remarkable structural similarity.[21,22,27,30] All three of these downstream effectors' Ras binding domains (RBD) share a ubiquitin-like fold and differ from each other by a RMSD of only ~2 Å for the Cα carbons.[16,23,24,31] What they share in overall fold is counter-balanced by the striking differences in sequence identity. Two of the most heavily investigated downstream effectors, Ral and Raf, share only a 13% sequence identity in the interfacing regions of the proteins,[20,31,32] although a large hydrophobic surface area common to Ras-association domains is preserved.[32] Given the remarkable structural similarity of these docked complexes, it is possible that electrostatic fields generated at the Ras–effector interface are the primary mechanism by which Ras can choose and bind to individual downstream effectors. This makes Ras an ideal candidate for studying the magnitude and molecular-level mechanism that electrostatic fields play in organizing these protein–protein complexes, while controlling for structural contributions to interface formation to the greatest extent possible.

Ral is a well-characterized protein whose interactions with WT Ras and mutants have been of interest to the community for some time.[16,27,31] Previously, our laboratory has studied the effector region of Ras using nitrile VSE probes introduced on Ral, and coupling VSE experiments and molecular dynamics simulations.[4,5] In the current report, we investigate this protein–protein interface from an alternative perspective, VSE probes located on the GTPase Ras, through a combination of spectroscopy and computational modeling. Mutations were made to nine residues on the surface of Ras that become immersed in the interface formed between Ras and Ral in the docked complex. The amino acids selected for placement of the nitrile vibrational probe at the Ras–Ral interface are shown in Fig. 1. Each of these amino acids was mutated to cysteine, then reacted to form the thiocyanate side chain. The absorption energy of each nitrile probe was measured on monomeric Ras. The nitrile-labeled Ras was then incubated with WT Ral, and changes in the absorption energy of each nitrile were measured through Fourier transform infrared (FTIR) spectroscopy.

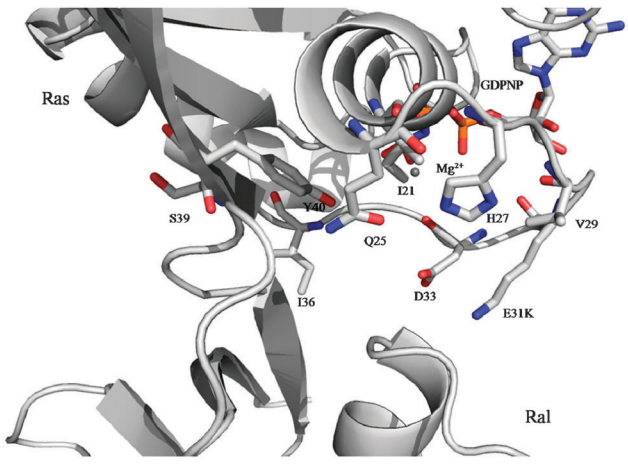


**Fig. 1** Structure of Ras docked with the RBD of Ral from crystal structure 1LFD,[31] identifying the positions of nine residues at the surface of Ras that were selected for mutagenesis and investigation by VSE spectroscopy and MD sampling. Also shown are GDPNP and $Mg^{2+}$ in the active site of Ras.

 

Enhanced molecular dynamics simulations employing an umbrella sampling strategy were conducted on both the monomeric (nitrile-labeled Ras) and docked (nitrile-labeled Ras plus Ral) complexes to obtain a Boltzmann-weighted distribution of nitrile probe positions and orientations on each experimental construct. These molecular dynamics simulations were used to interpret how structural changes in the location and orientation of the thiocyanate vibrational probe influenced absorption energy measurements. Finally, these data were compared to a previously published and complementary study of electrostatic fields measured from the Ral side of the Ras–Ral docked complex. These experimental data provide new insight into the role that electrostatic fields play at stable protein–protein interfaces.

## Materials and methods

### A. Protein mutagenesis, expression, purification, and labeling

The pProEx-Htb expression vector containing wild-type H-Ras residues 1–166 was taken from a previous study in our laboratory.[4] The plasmid was selective for ampicillin resistance and contained a 6×-histidine tag linked to the N-terminal end of the Ras construct with a tobacco etch virus (TEV) protease site. Amino acid mutations were made *via* the Stratagene Quick change mutagenesis kit with PCR primers obtained through Sigma-Aldrich. The Ras construct contained three wild-type (WT) cysteine residues, C51, C80, and C118. These cysteines were mutated to alanines, generating a cys-less construct hereafter referred to as Rasβ. Nine residues at the surface of Ras that become immersed in the Ras–effector binding interface were identified from the crystal structure 1LFD:[31] I21, Q25, H27, V29, E31, D33, I36, S39, and Y40. These residues were individually mutated to cysteine to generate nine Rasβ mutants.

The single cysteine Rasβ plasmids were transformed into competent BL21(DE3) *Eschericia coli* cells (Novagen) for expression and purification as discussed previously,[4] with the minor change that all buffered solutions used during the purification contained 10% glycerol to help stabilize Ras solubility. After purification, the Rasβ mutants were loaded with the non-hydrolyzable GTP analog guanosine 5′-[β,γ-imido]triphosphate trisodium salt hydrate (GDPNP, Sigma) to maintain the protein in the GTP-bound ON state for effector binding. Yields for the Rasβ mutants were typically 15–20 mg protein per liter of growth media. WT Ral purification was carried out as described previously.[4] All experimental data was obtained in a buffer of 50 mM Tris pH 7.5, 100 mM NaCl, and 10% glycerol.

Each of the nine Rasβ mutants were chemically modified with a thiocyanate Stark probe as has been reported previously.[4] Three molar equivalents of bis-thionitrobenzoic acid (DTNB, Aldrich) were added to the protein and allowed to react for 12–16 hours at 4 °C. The reaction was monitored by increase in the absorbance of the side product, thionitrobenzoic acid, at 412 nm. After one molar equivalent of DTNB had reacted, three molar equivalents of potassium cyanide (KCN, Aldrich) were added to the solution. The reaction was carried out at room temperature, and again the thionitrobenzoic acid absorbance was monitored by UV absorbance at 412 nm until completion, typically 2–4 h. The protein was then exchanged into fresh buffer consisting of 50 mM Tris pH 7.5, 100 mM NaCl, and 10% glycerol using a pd-10 desalting column (GE Healthcare). Herein we identify each thiocyanate-labeled Rasβ mutant with the subscript "SCN". The protein was then concentrated to 2 mM by centrifugation for infrared spectroscopy studies.

### B. Vibrational Stark effect spectroscopy

Vibrational absorption energy measurements were collected at room temperature in a sample cell comprised of two sapphire windows separated by 125 μm spacers in a Bruker Vertex 70 Fourier transform infrared spectrometer. The scan range was 2000 to 2500 $cm^{-1}$, selected by a band pass filter and collected on a liquid nitrogen cooled indium antimonide (InSb) detector. Each spectroscopic sample was obtained through 250 scans with a resolution of 0.5 $cm^{-1}$. Background samples were obtained using the same buffer solution without the protein. The background-subtracted absorption peak was fit using a custom least-squares fitting routine that has been described before to determine the absorption energy, $\nu_{obs}$.[33] Experimental error was calculated as the standard deviation of at least 5 replicates of spectroscopic sampling. Docked protein complexes were obtained by adding 1.3 molar equivalents of WT Ral to the labeled Ras mutant, equilibrating for two hours, and collecting infrared spectra according to the same experimental procedure used to obtain the vibrational spectra of each mutant.

### C. Binding dissociation constant assays

The dissociation constant, $K_d$, of docking of both WT Ras and each Rasβ mutant with WT Ral was determined using the guanosine dissociation inhibition (GDI) assay that has been described before.[4,33] Varying concentrations of WT Ral were incubated with 100 nM of the appropriate Ras construct loaded with a fluorescently-labeled GTP analog, 2′-(or 3′)-*O*-(*N*-methylanthraniloyl) guanosine 5′-triphosphate trisodium salt (mant-GTP, Invitrogen) for 2–16 hours at 4 °C in a top reading 96 well-plate (Microfluor). Mant-GTP dissociation was stimulated by the addition of 250 mM GDPNP along with gentle pipetting for 10 seconds to insure adequate mixture of the solution. Fluorescence decay was monitored in a multimode fluorometer (Beckman Coulter Spectra Max M3) using top-down intensity. Excitation and emission wavelengths were set to 365 nm, and 450 nm respectively, with a 2 s delay time between measurements. The initial decay in fluorescence intensity was fitted by least squares to determine $k_{obs}$, which was then used in eqn (2) to determine $K_d$,

$$k_{obs} = k_{-1} - k_{-1} \times \frac{(R_0 + E_0 + K_d) - \sqrt{(R_0 + E_0 + K_d)^2 - 4R_0E_0}}{2R_0} \quad (2)$$

where $R_0$ and $E_0$ are the known concentrations of the Ras construct and WT Ral, respectively, and $k_{-1}$ is the rate constant of the release of mant-GTP without the addition of WT Ral, determined by fitting the fluorescence decay data to a first-order exponential.

### D. Molecular dynamics and umbrella sampling

An *in silico* model of Rasβ was constructed using methods described previously.[4,5] This model contained the five N-terminal residues (GAMGS) that are not shown in the crystal structure 1LFD[31] but are present on the Rasβ construct after cleavage of the histidine affinity tag during protein purification. This model also contained the WT residue Glu31 instead of Lys31, which was used to crystallize Ras with Ral in crystal structure 1LFD. The mutations K31E, C51A, C80A, and C118A were accomplished using the tleap utility in AMBER tools.[4,34] Finally, nine models containing a single cyanocysteine residue at positions I21, Q25, H27, V29, E31, D33, I36, S39, or Y40 were generated by mutating the appropriate residue to a methionine (which contains the same number of heavy atoms as a cyanocysteine residue) using tleap.[34] The methionine mutation was then subsequently mutated to a cyanocysteine by editing the PDB file. The newly constructed mutants were each subjected to energy minimization by 100 steps of steepest-descents calculation using the GROMACS utility mdrun.[35] The $\chi_2$ torsion around the Cα and Sγ atoms on each cyanocysteine was rotated in increments of 60° for each of the nine mutants. The resulting 54 models were subjected to further vacuum energy minimization by 100 steps of steepest-descents calculations, and were considered the starting structures of our MD simulations. The 54 energy-minimized structures were placed in a dodecahedral simulation box filled with explicit TIP3P water molecules,[36] sodium ions were added to the box to give the overall model a neutral charge, and a final 5000 step steepest-descent energy minimization was run on the system. The solvent was then allowed to equilibrate for 10 000 2 fs steps by restraining the protein atoms with a harmonic potential of 1000 kJ $nm^{-1}$ $mol^{-1}$ in the three Cartesian directions.[4,5] After solvent equilibrations, three nanosecond simulations were carried out as discussed previously with two minor exceptions:[4] (1) the simulations were run on the Ranger supercomputer from Texas Advanced Computing Center using a 16 processor distribution; and (2) hydrogen bonds were restrained using the LINCS restraint rather than SHAKE, to allow for multiprocessor calculations.[35] The six $\chi_2$ torsions centered on 0°, 60°, 120°, 180°, 240°, and 300° were biased with a dihedral restraint potential that was flat within 45° and increased to 1000 kJ $mol^{-1}$ $rad^{-2}$ outside of that range. Each of the six starting torsions was run for three consecutive 1 ns trajectories, resulting in 18 ns of total sampling time for each monomeric Ras construct.

Simulations of each Ras–Ral docked construct were carried out in a similar manner using the molecular models of Ras docked with WT Ral built for a previous study.[4,5] The initial structure for docked simulations was obtained by aligning the Ras construct of interest with the Ras E31K mutant in 1LFD, and aligning WT Ral with the extended N-terminal and C-terminal tails with the Ral structure in 1LFD. Trajectories biased along $\chi_2$ were then done as described exactly for the monomeric simulations with the new docked models.

The Boltzmann weighted distribution of the $\chi_2$ dihedral for the cyanocysteine was calculated using a weighted histogram analysis method (WHAM) on the full 18 ns trajectories of both the monomer and docked complexes as described earlier.[5] The Boltzmann-weighted probabilities of $\chi_2$ from the final two thirds of simulation (6–18 ns) were compared to the first one third of the simulation (0–6 ns) to confirm that the simulation had converged through this sampling strategy.

### E. Azimuthal and polar angle calculations

The position of the nitrile on each cyanocysteine mutant was quantified according to its angle with respect to the Ras–Ral binding plane (azimuthal angle, $\phi$) and the center of mass of the monomeric or docked protein (polar angle, $\theta$). Methods for determining the binding plane, binding axis, polar axis, azimuthal angle, and polar angle have previously been discussed in detail.[5] The orientation of the bond vector pointing from the carbon to the nitrogen in the nitrile was determined from calculating the Boltzmann-weighted azimuthal and polar angles from the 18 ns simulations of each construct. A plane was constructed between the interfacial regions of the two proteins in the docked complex by calculating a least squares fit of the α-carbons on residues 20, 28–31, 32, and 33 on Ras, and residues 18, 20, 27–30, 52 and 54 on Ral from pdb input 1LFD. This plane is referred to as the surface plane. The azimuthal angle, $\phi$, was defined as the elevation above or below this plane. The polar angle, $\theta$, was taken to be the rotation about an axis that was orthogonal to the surface plane, defined as the polar axis.

## Results

### A. Dissociation constant of Ras constructs with WT Ral

Assessing the extent of changes induced into the system through mutation and chemical labeling is necessary to understand the perturbations to the Ras–Ral docking that might occur due to the experimentally introduced thiocyanate vibrational probe. To address this, dissociation constants, $K_d$, for each of the nine SCN-labeled Rasβ mutants docking with WT Ral were measured and compared to the value for WT Ras ($3.5 \pm 0.3$ μM). These results are given in Table 1, and show that with the exception of Ras $E31C_{SCN}$ and $D33C_{SCN}$, the presence of the thiocyanate probe causes essentially no deviation in the

**Table 1** Binding kinetics of WT Ras and each of the Rasβ mutants docked with WT Ral

| Ras mutant | $K_d$[a] (μM) |
|---|---|
| WT | $3.5 \pm 0.3$ |
| Rasβ $I21C_{SCN}$ | $5 \pm 1$ |
| Rasβ $Q25C_{SCN}$ | $4.3 \pm 0.4$ |
| Rasβ $V29C_{SCN}$ | $5.5 \pm 0.4$ |
| Rasβ $H27C_{SCN}$ | $5.5 \pm 0.6$ |
| Rasβ $E31C_{SCN}$ | $12.3 \pm 0.2$ |
| Rasβ $D33C_{SCN}$ | $17 \pm 3$ |
| Rasβ $I36C_{SCN}$ | $4.4 \pm 0.2$ |
| Rasβ $S39C_{SCN}$ | $7.0 \pm 0.6$ |
| Rasβ $Y40C_{SCN}$ | $4.4 \pm 0.7$ |

[a] Dissociation constants were obtained by fitting $k_{obs}$ from the GDI assay to eqn (2). Errors are reported as one standard deviation of at least three experimental replicates.

 

rate of docking compared to the WT system. Ras D33 has been shown to be important for determining docking specificity[37] between Ras and Ral *in vitro* by participating in an extended hydrogen bonding network that stabilizes the formation of the protein–protein complex, and so it is not unreasonable for the Ras $D33C_{SCN}$ mutation to cause the observed 5-fold increase in $K_d$.[16,31] The sensitivity of the $K_d$ to mutations at Ras E31 is somewhat more surprising. An unrelated GTPase, WT Rap, contains a lysine at position 31, and binds to WT Ral with a $K_d$ approximately an order of magnitude lower than the interaction between WT Ral and WT Ras. We have previously shown that the mutation Rap K31E converts both the kinetics and electrostatics of binding between GTPase and Ral to the behavior of WT Ras.[33] By analogy, mutation of Rap E31 to an uncharged cysteine mutation should remove unfavorable electrostatic repulsions from this region of the interface and promote the docking interaction. We believe this result is explained with a comprehensive analysis of all VSE data available at the Ras–Ral interface, and so will return to this observation below. However, even with these complications, the increase in $K_d$ caused by placing the thiocyanate probe at these locations was less than a factor of five even in the most perturbed case, indicating that binding was not abolished between the two proteins, and that in a steady-state experiment at least approximately 96% of the sample remained in the docked configuration. The kinetic data are thus strong experimental evidence that introduction of the small thiocyanate probe does not significantly alter the protein–protein interface under investigation, and that our spectroscopic measurements are being conducted on a system that is substantially representative of the WT interactions in which we are interested.[38]

### B. Simulations of the thiocyanate probe on the surface of Rasβ

Stable protein–protein interactions are formed from the interplay of two main factors: structural complementarity, which we include to mean hydrogen bonding, salt bridge formation, and hydrophobic effects; and electrostatic fields. To study in detail the role that electrostatics plays in protein–protein interactions, a VSE probe was placed at nine positions on Ras at the interface formed between Ras and Ral described by the 2.1 Å resolution crystallographic structure of Ras E31K bound to WT Ral.[31] Since the effect of a local electrostatic field on the absorption energy of the vibrational probe is proportional to the projection of the field vector onto the nitrile bond axis, in order to interpret vibrational absorption data as an electrostatic field it is necessary to estimate the average orientation of the VSE probe with respect to the binding interface. We therefore used molecular dynamics simulations employing an umbrella sampling strategy to determine the Boltzmann-weighted torsional distribution of the $\chi_2$ angles for the cyanocysteine side chain on both the SCN-labeled Rasβ monomers and in the docked Rasβ–Ral complex. Probability distributions for the $\chi_2$ angle of the cyanocysteine on each SCN-labeled Rasβ mutant in both monomeric (red) and docked (blue) configurations are shown in Fig. 2. Each of the nine sampled thiocyanate torsions have probability maxima at approximately $\pm60^\circ$, $\pm120^\circ$, and $\pm180^\circ$, and are thus predictably alkane. (Probability maxima that appear at $\pm30^\circ$ are most likely artifacts of the torsional biasing during MD simulation, which employed a 30°-wide flat well for umbrella sampling.) We also observed little change in the $\chi_2$ distribution between monomeric and docked SCN-labeled Rasβ complexes, and in no case did formation of the protein–protein interface cause significant distortion of the alkane-like nature of the cyanocysteine side chain. Dihedral angle probability distributions were determined for the first 6 ns and were compared to the probability distributions determined during the last 12 ns of simulation. There was no significant difference between these two distributions (data not shown), suggesting that the simulations had achieved convergence for the dihedral orientation and have generated a Boltzmann-weighted statistical ensemble of the most probable orientations of the nitrile with respect to the $\chi_2$ dihedral angle of the cyanocysteine side chain. These Boltzmann-weighted probability distributions then become the basis for calculating Boltzmann-weighted averages of other spatially relevant attributes of the thiocyanate probe in three-dimensional space.

Using these statistical ensembles of thiocyanate orientations, we measured the orientation of the thiocyanate with respect to the protein–protein interface based on an azimuthal ($\phi$) and polar ($\theta$) angle polar coordinate.[4] The azimuthal angle was defined as the angle of elevation of the VSE probe with respect to a plane formed at the binding interface, shown schematically in Fig. 3, where the SCN-labeled Rasβ mutant is located above the surface plane (*i.e.* the $\phi = 0^\circ$ axis), while Ral is below the surface plane. Results for both the monomer (red) and docked (blue) SCN-labeled Rasβ-WT Ral complexes are given in Fig. 4. In all cases, the probe pointed outward to the solvent on the monomer, and in most cases remained in this orientation upon binding to WT Ral. However, mutants Rasβ $D33C_{SCN}$ and Rasβ $S39C_{SCN}$ both show a preferential shift away from Ral and towards the interior of Rasβ upon docking with WT Ral. By examining representative snapshots along our sampling trajectory, it was apparent that the change in the Rasβ $S39C_{SCN}$ azimuthal angle upon docking was caused by the steric clashes between the thiocyanate and the bulky side chain of Ral Y28 that is introduced upon docking. This resulted in a change of 60° in the $\chi_1$ angle for the thiocyanate to point upwards into the interior of Ras. The cause for the change in Rasβ $D33C_{SCN}$ orientation appeared to be from the flexibility of the so-called ''switch I'' loop (residues 31–40) that has a small but significant structural difference between the monomer and the docked complex (measured as a RMSD of 0.48 Å in X-ray structures comparing monomeric and docked states).[31] This was replicated in an observed RMSD of approximately 0.5 Å in this region during the simulation when comparing the Cα backbone atoms for monomer and docked complexes, and indeed, the calculated variance for the cyanocysteine side chain (shaded regions in Fig. 4) was largest at Rasβ $D33C_{SCN}$ compared to other probe locations. However, in general, variance for each azimuthal angles on both monomeric and docked complexes remained quite low ($<\pm13^\circ$), did not display any systematic behavior, and do not appear to be correlated in any

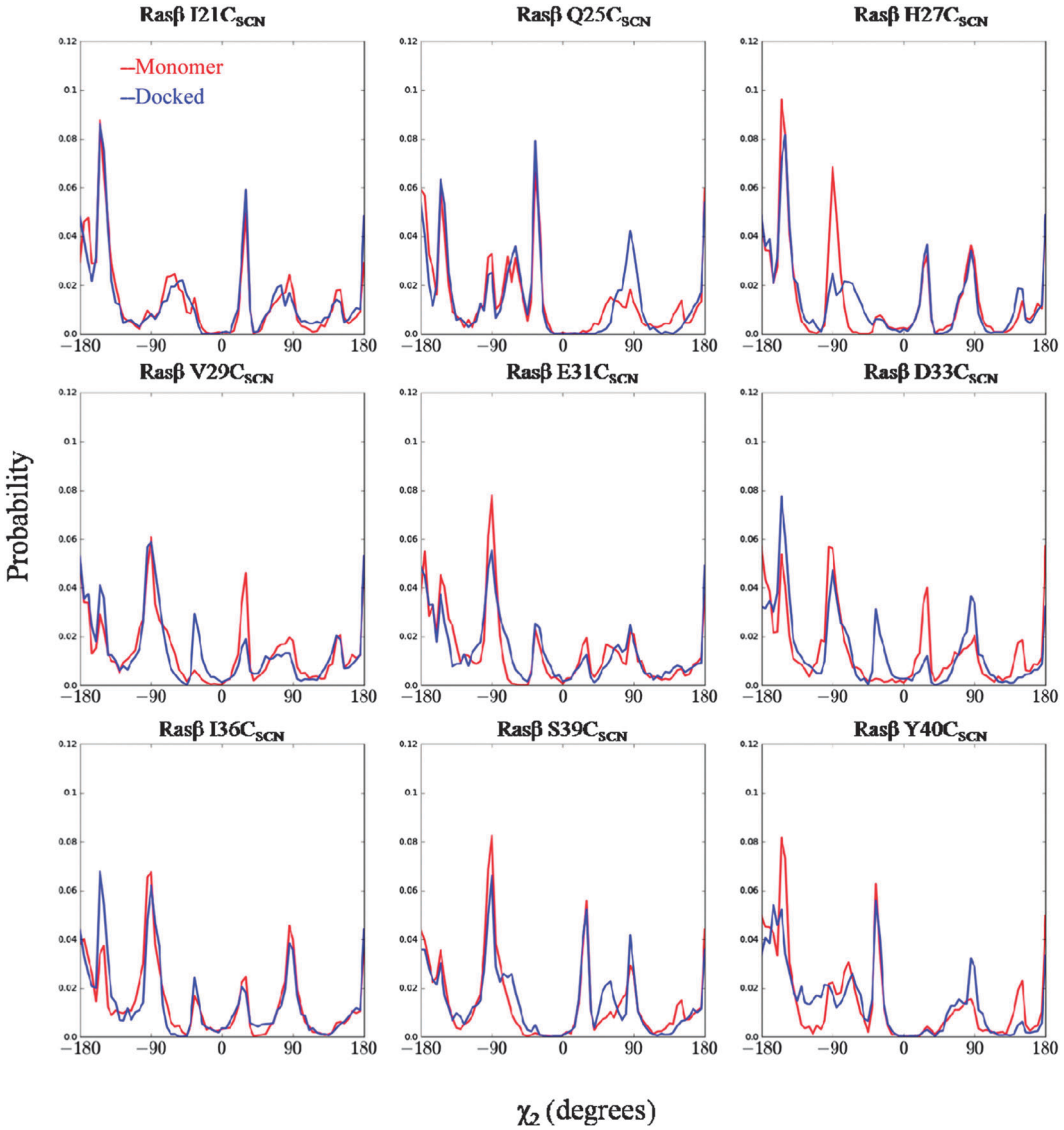


**Fig. 2** Boltzmann-weighted torsional probability distributions of the $\chi_2$ dihedral of the cyanocysteine for the monomeric Rasβ protein (red), and docked to WT Ral (blue). Each distribution represents 18 ns of sampling at 300 K in explicit TIP3P waters.

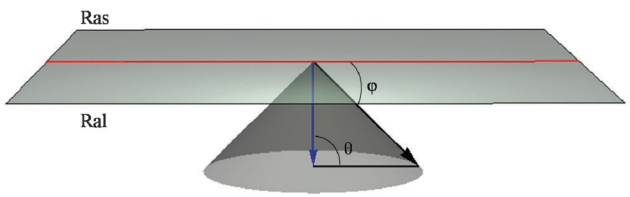


**Fig. 3** Representations of the azimuthal and polar angles. The azimuthal angle, $\phi$, is a measurement of the elevation from the binding plane between the proteins. The polar angle, $\theta$, is a measurement of rotation about polar axis depicted as a blue line orthogonal to the binding axis shown in red.

way with vibrational absorption energy of the thiocyanate, discussed below.

Another measure of the position of the thiocyanate probe with respect to the protein surface is given by the thiocyanate's solvent accessible surface area (SASA), a measure of how much of the probe is exposed to water based on its orientation at the protein surface. The SASA for the entire cyanocysteine residue was calculated from the Boltzmann-weighted ensemble of structures for both monomeric and docked complexes using the Gromacs utility g_sas, and are given in Table 2.[35] These residues were chosen for our studies because of their solvent-accessible location on the binding interface of Rasβ, and we have measured SASA values as high as 140 Å$^2$ for similarly placed solvent-accessible nitrile probes in other protein constructs in our laboratory.[4] However, the SASA values we measured in were relatively small, 20 to 60 Å$^2$, and did not decrease significantly upon docking with WT Ral. These results indicate that most residues are being excluded from water on the surface of the Rasβ monomer because of their orientation with respect to the protein surface. This is not surprising when considering the measured azimuthal angles shown in Fig. 4, which demonstrated that most cyanocysteine mutants lie nearly

 

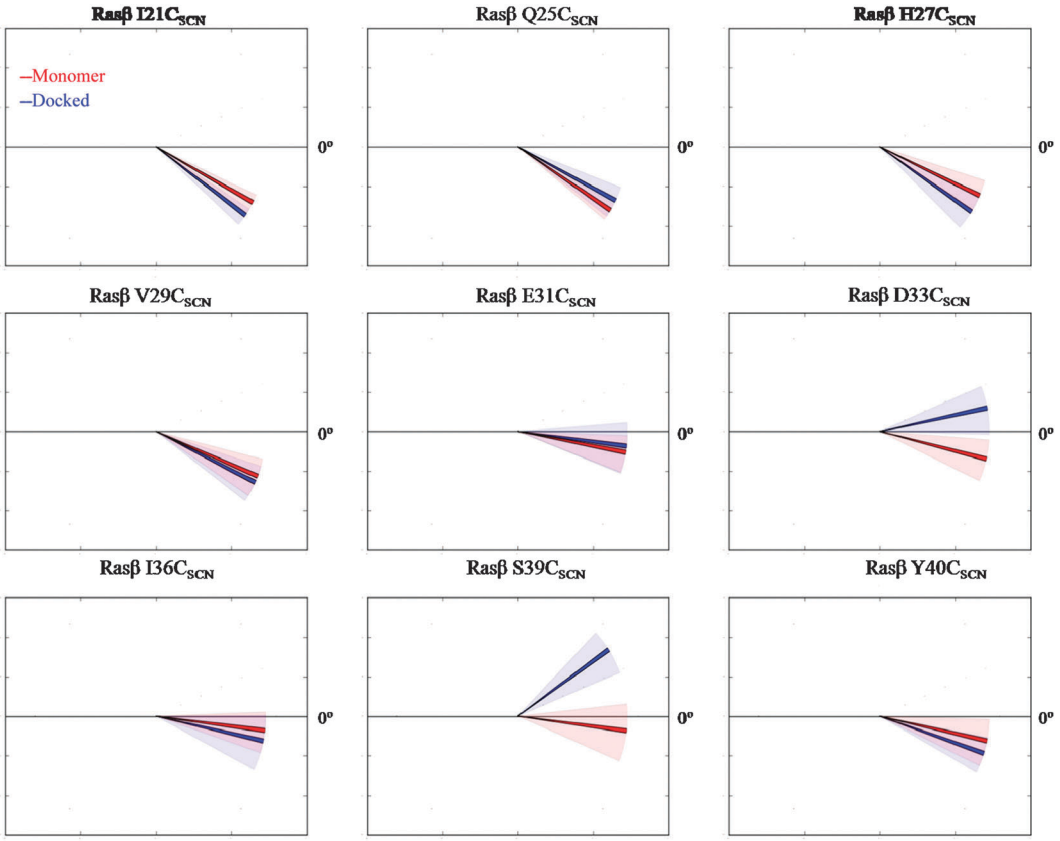


**Fig. 4** Boltzmann weighted averages of the azimuthal angle made from the nitrile bond in the thiocyanate to the binding plane between Rasβ and Ral. The ensemble averages are given as solid lines, with variance about the average shown by the shaded areas. Monomeric sampling is shown in red, and the docked sampling is shown in blue. In this view Ras is situated above the horizontal axis, and Ral is situated below the horizontal axis.

**Table 2** Solvent accessible surface area (SASA) calculations of both the monomer and docked complex of each Rasβ mutant[a]

| Mutants | Monomer SASA (Å$^2$) | Docked SASA (Å$^2$) |
|---|---|---|
| Rasβ I21C$_{SCN}$ | 20 ± 10 | 30 ± 10 |
| Rasβ Q25C$_{SCN}$ | 30 ± 10 | 20 ± 10 |
| Rasβ H27C$_{SCN}$ | 50 ± 10 | 40 ± 10 |
| Rasβ V29C$_{SCN}$ | 60 ± 10 | 60 ± 10 |
| Rasβ E31C$_{SCN}$ | 56 ± 9 | 40 ± 10 |
| Rasβ D33C$_{SCN}$ | 50 ± 10 | 50 ±10 |
| Rasβ I36C$_{SCN}$ | 40 ± 10 | 25 ± 9 |
| Rasβ S39C$_{SCN}$ | 50 ± 10 | 40 ± 10 |
| Rasβ Y40C$_{SCN}$ | 30 ± 10 | 15 ± 8 |

[a] Values calculated from the Boltzmann-weighted statistical ensemble of thiocyanate $\chi_2$ torsion angles. The error reported is one standard deviation obtained from the Boltzmann-weighted conformational sampling.

parallel to the interface in both the monomeric and docked complexes. Taken as a whole, these low measured SASA values for each mutant suggest that differences in absorption energies of the monomer are derived from electrostatic fields being generated by the protein itself rather than being dominated by interactions with water such as hydrogen bonding.[4,5,14,39]

An additional metric of the orientation of the thiocyanate probe with respect to the Rasβ–Ral interface is the angle of rotation of the probe about an axis orthogonal to the binding interface; we refer to this angle as the polar angle, $\theta$. This angle represents the degree of conformational variability of the probe with respect to the center of mass of the protein and parallel to the binding interface. Because the position of the residue with respect to the center of mass is different for each nitrile location, Fig. 5 is given to aid in visual

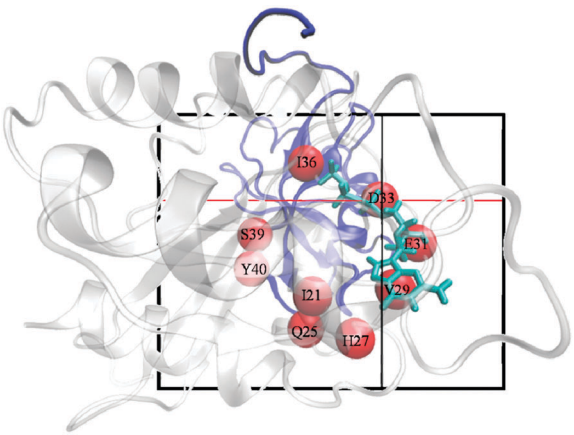


**Fig. 5** Representation of the polar angle for each Rasβ mutant. Ras is shown as transparent white, the position of the Cα atoms of each cyanocysteine residue are shown as red spheres, and Ral is shown in blue. The polar angle can be visualized by translating the axis origin of the crosshairs to the center of each sphere (radius of the spheres are not shown to scale).

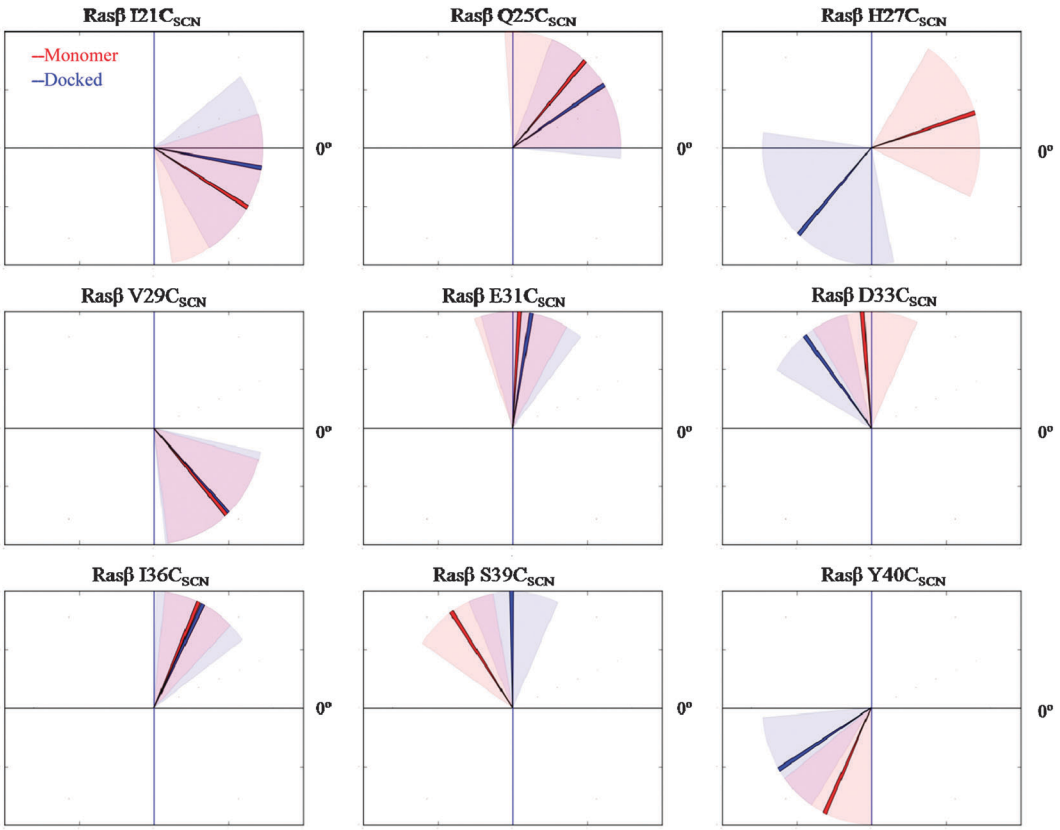


**Fig. 6** Boltzmann-weighted averages of the polar angle between Ras and Ral made between the polar axis shown in blue to the nitrile bond in the cyanocysteine side chain. Monomeric sampling is shown in red, and the docked sampling is shown in blue. The ensemble averages are given as solid lines, with variance about the average shown by the shaded areas.

interpretation of results for the polar angle. When the cross-hairs of the axes shown in Fig. 5 are translated to the center of each spherical Cα atom they become the origin for $\theta$. These results are shown in Fig. 6 for both monomeric (red) and docked (blue) complexes. The measured value of $\theta$ varied considerably depending on the location of the cyanocysteine mutant with respect to the center of mass of the protein, and therefore on its location around the protein interface. Although there was a greater variability in this measurement between the monomeric and docked complexes than seen for $\chi_2$ torsional angles or azimuthal angles (measured as a variance and shown as the shaded regions on Fig. 6), at only one position, Rasβ H27C$_{SCN}$, did protein–protein docking cause the cyanocysteine side chain to assume a significantly different orientation. Careful examination of representative snapshots taken during the MD trajectory indicate that this change of $\sim 130^{\circ}$ between the monomeric and docked complexes was caused by a steric clash between the thiocyanate and the bulky side chain of WT Ral L52, forcing the $\chi_2$ orientation of H27C$_{SCN}$ to rotate approximately $40^{\circ}$ from its position in the Ras monomer. This small dihedral change, which did not disrupt the alkane-like nature of the side chain, is magnified when viewed relative to the polar axis that is orthogonal to the surface plane, which is the value measured by $\theta$. The result is a large shift if the polar angle of the thiocyanate upon docking. In no case was the variance in $\theta$ correlated with vibrational absorption energies of the thiocyanate probes, discussed below.

### C. Vibrational Stark effect spectroscopy

Investigations of the binding interface are shown in Table 3 and in Fig. 7 and 8. Fig. 7 is a representative of the two normalized vibrational spectra of Rasβ I36C$_{SCN}$ monomer and docked with Ral. Two prominent features of the spectrum are the decrease in absorption energy and a slight narrowing of the peak width caused by docking of the I36C$_{SCN}$ mutant to WT Ral. The uniform Gaussian symmetry in both spectra indicate that we are observing a steady-state interaction between the two proteins. The low variance in both $\phi$ (Fig. 4) and $\theta$ (Fig. 6) for the probe in Rasβ I36C$_{SCN}$ confirm that this cyanocysteine populates one configuration in the monomeric protein and that its orientation in the complex does not change significantly upon docking with WT Ral. The absorption energy of the thiocyanate probe on all monomeric Rasβ constructs, shown in Fig. 8A and reported in Table 3, varied over 4 cm$^{-1}$ (2159.0–2162.9 cm$^{-1}$); each individual position was measured to a standard deviation of at least $<0.6$ cm$^{-1}$ and usually smaller. Taken together with the SASA results discussed above, this suggests that although all of these probes are on the surface of the protein of the Rasβ monomer, these thiocyanates are relatively sequestered from solvent by the surface of the protein.[4]

 

**Table 3** Comparison of the vibrational absorption energies of each of the nine SCN-labeled Rasβ mutants in both monomeric and docked complexes[a]

| | Monomer | | Docked with WT Ral | | |
|---|---|---|---|---|---|
| Mutants | $\nu_{obs}$ ($cm^{-1}$) | fwhm ($cm^{-1}$) | $\Delta\nu_{obs}$ ($cm^{-1}$) | Δfwhm ($cm^{-1}$) | $\Delta\vec{F}_{protein}$ (MV $cm^{-1}$) |
| Rasβ $I21C_{SCN}$ | 2161.2 ± 0.4 | 11.6 ± 0.3 | −0.42 ± 0.5 | −1.0 ± 0.5 | 0.6 |
| Rasβ $Q25C_{SCN}$ | 2160.0 ± 0.6 | 12.0 ± 0.5 | −1.2 ± 0.6 | −0.8 ± 0.6 | 1.7 |
| Rasβ $H27C_{SCN}$ | 2160.5 ± 0.3 | 11.7 ± 0.6 | −1.27 ± 0.9 | −1.2 ± 0.9 | 1.8 |
| Rasβ $V29C_{SCN}$ | 2161.1 ± 0.1 | 13.6 ± 0.2 | −0.9 ± 0.4 | −1.1 ± 0.4 | 1.3 |
| Rasβ $E31C_{SCN}$ | 2161.3 ± 0.3 | 12.4 ± 0.3 | −2.8 ± 0.4 | −0.4 ± 0.4 | 4 |
| Rasβ $D33C_{SCN}$ | 2161.7 ± 0.2 | 14.3 ± 0.7 | 0.9 ± 0.4 | −0.2 ± 0.6 | −1.3 |
| Rasβ $I36C_{SCN}$ | 2162.9 ± 0.4 | 11.8 ± 0.3 | −1.2 ± 0.5 | −1.4 ± 0.5 | 1.7 |
| Rasβ $S39C_{SCN}$ | 2160.8 ± 0.4 | 12.5 ± 0.8 | 0.6 ± 0.2 | −0.7 ± 0.3 | −0.9 |
| Rasβ $Y40C_{SCN}$ | 2159.0 ± 0.2 | 13.7 ± 0.6 | 1.0 ± 0.5 | −0.9 ± 0.5 | −1.4 |

[a] The error reported is one standard deviation of at least three experimental replicates.

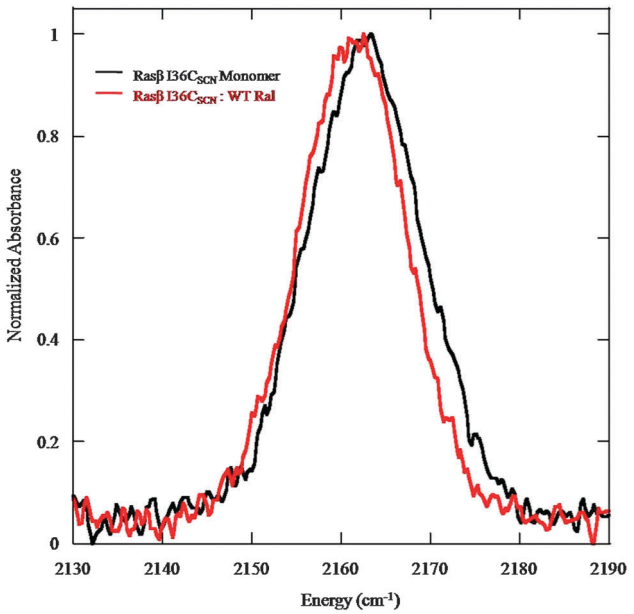


**Fig. 7** Representative spectra of the monomeric Rasβ $I36C_{SCN}$ (black) and Rasβ $I36C_{SCN}$ docked with WT Ral (red). The absorption energy of the nitrile at this position decreases by ~1 $cm^{-1}$ upon docking with WT Ral compared to the monomeric state.

We have previously measured the absorption energy of the nitrile frequency in methyl thiocyanate (MeSCN) to be 2162.1 ± 0.1 $cm^{-1}$ in our buffer containing 10% glycerol. This represents the absorption of the nitrile under fully solvent-exposed conditions, when the nitrile is mostly likely acting as a hydrogen bond acceptor from the protic solvent.[40,41] Because of convolutions of hydrogen bonding and electrostatic effects, this is therefore a complication when attempting to interpret vibrational absorption energy.[14] Furthermore, we measured MeSCN in 100% tetrahydrofuran (THF) in 2 mM concentrations. The absorbance in the aprotic environment while solvated in THF was 2157.5 ± 0.1 $cm^{-1}$. The fact that eight of the nine cyanocysteine mutants studied here had absorption energies less than the absorption energy of MeSCN in aqueous solution is further evidence that these probes are not interacting with water to any great extent. The one exception to this observation, Rasβ $I36C_{SCN}$, with an absorption energy in the monomeric form of 2162.9 ± 0.4 $cm^{-1}$, also showed the largest decrease in SASA going from the monomeric to docked complexes, 40 $Å^2$ and 25 $Å^2$, respectively. This is expected if the side chain is exposed to water that is then displaced when the protein–protein complex is formed. The vibrational absorption results and MD simulations thus both support the conclusion that with the possible exception of Rasβ $I36C_{SCN}$, these nitrile probes are not participating in extensive hydrogen bonding interactions with water in either the monomeric or docked complexes, and that therefore they are useful probe positions for investigating the magnitude and function of electrostatic fields at the Ras–Ral interface.

After the absorption energy of the SCN-labeled Rasβ monomer was measured, the protein was then incubated with WT Ral and the absorption energy of the thiocyanate was measured in the docked complex. The results showing the change in absorption energy between the monomeric and docked complexes, $\Delta\nu_{obs}$, are described in Table 3 and Fig. 8B. Six of the nine mutants experienced a lower absorption energy in the docked complex *versus* the monomer, while the remaining three experienced an increase in absorption energy. The change in absorption energy ranged from −2.8 ± 0.4 $cm^{-1}$ to +0.9 ± 0.4 $cm^{-1}$, representing a change in electrostatic field of over 5 MV $cm^{-1}$ (+4.0 to −1.3 MV $cm^{-1}$, eqn (1)) depending on the location of the nitrile probe. Interestingly, two of the three mutant locations that experienced an increase in absorption energy upon docking, Rasβ $D33C_{SCN}$ and Rasβ $S39C_{SCN}$, were the only two mutants to experience a large change in the azimuthal angle, $\phi$, from the monomeric to docked complexes. In both cases, the cyanocysteine side chains at these locations moved from relatively near the surface of the Rasβ protein to above the Rasβ–Ral surface plane, showing that these side chains were sequestered inside the Ras-side of the interfacial area formed by the docked complex. The full width at half maximum (fwhm) decreased upon effector binding for each probe, sometimes significantly (~−1.0 $cm^{-1}$ for seven if nine of the studied mutants), but this was not correlated to $K_d$ measurements or MD sampling in any way.

## Discussion

If electrostatic fields are an important mechanism for the formation and function of stable and specific protein–protein interactions, then docking partners will have to recognize each

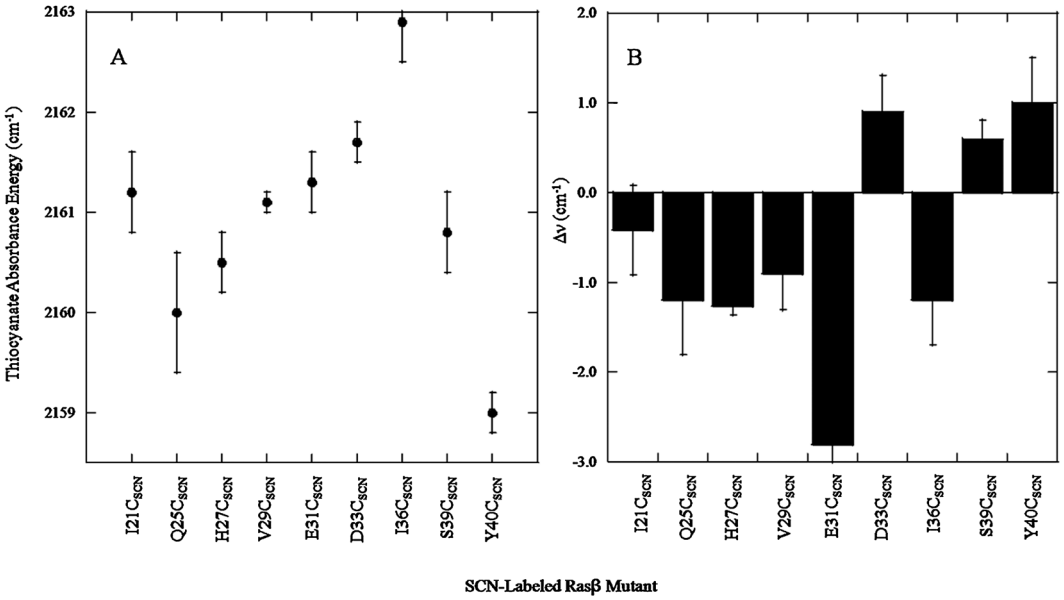


**Fig. 8** (A) Absorption energies of each of the nine monomeric Rasβ probes. (B) The measured spectral change to the thiocyanate probe for each Rasβ mutant binding to WT Ral. All spectra were collected in a solution of 50 mM Tris pH 7.5, 100 mM NaCl, and 10% glycerol.

other through a pattern of weak but long-range electric fields across the docking surface. When rationalizing the structure of docked complexes, many researchers point to the apparent matching of complementary electrostatic fields to justify why a single thermodynamic orientation is selected over a large number of possibilities.[42] The surface area of the Ras–Ral interface is approximately 1500 Å$^2$; systematically probing the electrostatic environment along this large interface allows us to test whether selecting for electrostatic complementarity is a plausible mechanism for orienting the two proteins into their observed configuration in the docked complex. The study reported here, employing nine nitrile probes along the Rasβ–Ral interface, is complementary to a previously published report in which nine thiocyanate probes were placed along the Ral surface, then docked with WT Ras.[4] The present results can therefore be combined with published data to create a global perspective of the role of electrostatic fields in this specific docking interaction.

Because we have now investigated this interface from the perspective of both of the proteins in the complex, it is instructive to compare results from thiocyanate probes introduced from two different proteins but sitting at the same position of the protein–protein interface and interacting with residues from the other protein. This is most easily seen when the direction of the energy shift of the thiocyanate absorption (higher or lower energy) *versus* the absorption energy in buffer is superimposed on the structure of the docked complex itself. In Fig. 9, positions of the protein surface where the nitrile probe experienced $\Delta\nu_{obs} < 0$ are shown in red, while positions that resulted in $\Delta\nu_{obs} > 0$ are shown in blue, compiled both from the data in Table 3 and the data in Table 2 of Stafford, *et al.*[4] In Fig. 9A, this interface is shown side-on, where transparent red surfaces allow us to visualize the blue interior of the interface. In Fig. 9B, these same data are shown looking

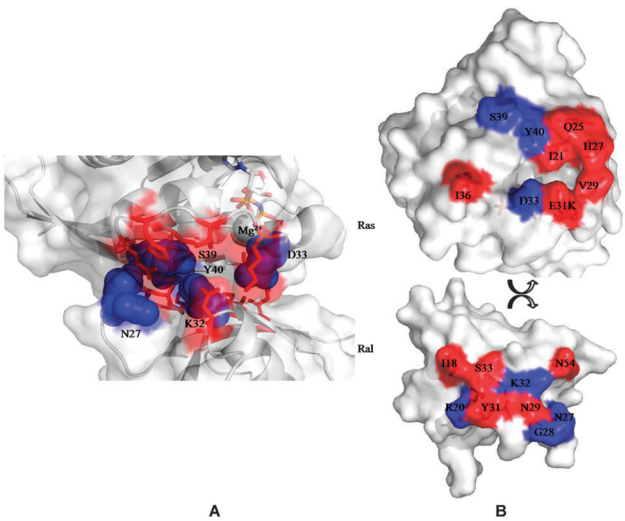


**Fig. 9** (A) Side view of the Ras–Ral interface. The direction of the energy shift of the nitrile at each position is indicated by blue (higher energy) and red (lower energy) labels. Transparent white surfaces represent the exterior of the protein surface. (B) View of the interface of Ras (top) and Ral (bottom) showing the position of each residue discussed here. Blue and red labels represent shifts in the nitrile's vibrational frequency upon docking to higher (blue) or lower (red) energy.

onto the protein surfaces in the formed interface. This comprehensive data set, describing a large number of individual experiments of a nitrile probe moved systematically with Ångstrom resolution around the protein–protein interface, shows a distinct pattern of interacting residues based on their position in the protein–protein complex. Thiocyanate probes on the surface of Rasβ demonstrated a distinct pocket in which the thiocyanate absorption energy shifted to higher energy, defined by the residues D33C$_{SCN}$, S39C$_{SCN}$, and Y40C$_{SCN}$. This pocket surrounds

 

Ralβ K32$C_{SCN}$, which also experiences a blue shift moving from the monomeric to docked complexes. This pocket of $\Delta\nu_{obs} > 0$ (and thus $\Delta\vec{F}_{protein} < 0$) is completely surrounded by a ring of residues that all had measured $\Delta\nu_{obs} < 0$ (and thus $\Delta\vec{F}_{protein} > 0$) from both proteins: Rasβ I21$C_{SCN}$, Q25$C_{SCN}$, H27$C_{SCN}$, V29$C_{SCN}$, E31$C_{SCN}$, and I36$C_{SCN}$; and Ralβ I18$C_{SCN}$, N29$C_{SCN}$, Y31$C_{SCN}$, S33$C_{SCN}$, and N54$C_{SCN}$. This appears to create a pocket of electrostatic complementarity (blue) in the middle of a ring of alternate complementarity (red) in the formed Ras–Ral interface. This is exciting evidence that the role of electrostatic fields at this protein–protein interface includes a mechanism for orienting the two proteins in the correct positions for the function of the docked complex.

This complete view of electrostatic fields at the Ras–Ral interface helps explain two key observations, the increase in $K_d$ for the formation of the docked interfaces containing Rasβ E31$C_{SCN}$ and D33$C_{SCN}$, and the curious placement of the positively charged Ral K52 side chain near the $Mg^{2+}$ bound to the Ras active site. Fig. 9 shows clearly that Ras D33 is crucial for creating the electrostatic pocket that surrounds Ral K32 in the docked structure. This has previously been identified as a hydrogen-bonding interaction,[20,37] and without question that element of the structure contributes to the stability of the structure. However, Ras D33 is necessary to create the extended patch of electrostatic complementarity in the center of the docked interface that recognizes the contribution from Ral K32. Without this noncovalent interaction, the binding between Ras and Ral will become weaker and/or less specific for the particular orientation of Ras and Ral that leads to this specific configuration, both of which would cause an increase in the rate of dissociation of the docked complex. This also explains why the docked configuration places the positive charge of Ral K32 so near to the $Mg^{2+}$ ion complexed to GPDNP in the active site of Ras. This repulsive Coulombic interaction is mitigated by the pocket of electrostatic potential that has been created by the proximity of Ral K32 to Ras D33, S39, and Y40. Ras E31 appears to serve the same purpose of creating the ring of high $\Delta\vec{F}_{protein}$ (low $\Delta\nu_{obs}$, red) that surrounds the internal binding pocket. These details only become apparent or relevant once the global electrostatic field around the entire protein–protein interface has been mapped and investigated in its entirety.

In summary, we have systematically measured electrostatic fields along the interface of the human oncoprotein H-Ras when docked with the RBD of the downstream effector protein Ral. Molecular dynamics simulations demonstrate that the thiocyanate probes deployed along the surface of Ras are on average oriented approximately horizontal to the Ras–Ral interface, and thus are not likely to be engaged in extensive hydrogen bonding with solvent water molecules. When combined with an extensive data set previously obtained for a similar study on the surface of Ral, we have identified regions of electrostatic complementary created by the docked interaction between Ras and Ral that appear to be significantly responsible for creating this docked configuration. It must be emphasized that we can measure these electrostatic fields only at positions at which we can reliably place a nitrile probe, and only in orientations determined by the nitrile vector's orientation in three-dimensional space. Even though the selected SCN-labeled residues are near to or sequestered within the formed protein–protein interface, this does not guarantee that we have measured the full extent of all electrostatic contributions. Electrostatics calculations designed to test our hypotheses and kinetics experiments to measure the effect of mutations to these residues are underway in our laboratory and will be reported in a future study.

## Acknowledgements

This work was supported by the Burroughs Wellcome Fund (1007207.01) and The Welch Foundation (F-1722). L.J.W. holds a Career Award at the Scientific Interface from the Burroughs Wellcome Fund and is an Alfred P. Sloan Research Fellow. The authors acknowledge the Texas Advanced Computing Center (TACC) at The University of Texas at Austin for providing high-performance computing resources that have contributed to the results reported within this paper, as well as the Institute of Cellular and Molecular Biology at The University of Texas at Austin for use of the fluorimeter for kinetic studies.

## References

1 S. J. Wodak and J. Janin, *Adv. Protein Chem.*, 2003, **61**, 9–73.
2 H. Weinstein and R. Osman, *Neuropsychopharmacology*, 1990, **3**, 397–409.
3 J. Janin and R. P. Bahadur, *Cell. Mol. Bioeng.*, 2008, **1**, 327–338.
4 A. J. Stafford, D. L. Ensign and L. J. Webb, *J. Phys. Chem. B*, 2010, **114**, 15331–15344.
5 D. L. Ensign and L. J. Webb, *Proteins*, 2011, **79**, 3511–3524.
6 W. H. Hu and L. J. Webb, *J. Phys. Chem. Lett.*, 2011, **2**, 1925–1930.
7 S. S. Andrews and S. G. Boxer, *J. Phys. Chem. A*, 2002, **106**, 469–477.
8 S. S. Andrews and S. G. Boxer, *J. Phys. Chem. A*, 2000, **104**, 11853–11863.
9 G. U. Bublitz and S. G. Boxer, *Annu. Rev. Phys. Chem.*, 1997, **48**, 213–242.
10 M. M. Waegele, R. M. Culik and F. Gai, *J. Phys. Chem. Lett.*, 2011, **2**, 2598–2609.
11 E. S. Park, S. S. Andrews, R. B. Hu and S. G. Boxer, *J. Phys. Chem. B*, 1999, **103**, 9813–9817.
12 L. J. Webb and S. G. Boxer, *Biochemistry*, 2008, **47**, 1588–1598.
13 A. T. Fafarman, L. J. Webb, J. I. Chuang and S. G. Boxer, *J. Am. Chem. Soc.*, 2006, **128**, 13356–13357.
14 J. H. Choi and M. Cho, *J. Chem. Phys.*, 2011, **134**, 154513.
15 H. C. Lee, J. H. Choi and M. H. Cho, *J. Chem. Phys.*, 2012, **137**, 114307.
16 C. Herrmann and N. Nassar, *Prog. Biophys. Mol. Biol.*, 1996, **66**, 1–41.
17 V. Ayllon and A. Rebollo, *Mol. Membr. Biol.*, 2000, **17**, 65–73.
18 A. D. Cox and C. J. Der, *Oncogene*, 2003, **22**, 8999–9006.
19 J. Downward, *Nat. Rev. Cancer*, 2003, **3**, 11–22.

20 A. Wittinghofer and N. Nassar, *Trends Biochem. Sci.*, 1996, **21**, 488–491.
21 C. Block, R. Janknecht, C. Herrmann, N. Nassar and A. Wittinghofer, *Nat. Struct. Biol.*, 1996, **3**, 244–251.
22 S. L. Campbell, R. Khosravi-Far, K. L. Rossman, G. J. Clark and C. J. Der, *Oncogene*, 1998, **17**, 1395–1413.
23 J. Downward, *Nat. Med.*, 2008, **14**, 1315–1316.
24 J. Wang, Y. Z. Yuan, Y. Zhou, L. H. Guo, L. Q. Zhang, X. Z. Kuai, B. W. Deng, Z. Pan, D. Li and F. C. He, *J. Proteome Res.*, 2008, **7**, 3879–3889.
25 A. Mor and M. R. Philips, *Annu. Rev. Immunol.*, 2006, **24**, 771–800.
26 N. Berndt, A. D. Hamilton and S. M. Sebti, *Nat. Rev. Cancer*, 2011, **11**, 775–791.
27 C. Herrmann, G. Horn, M. Spaargaren and A. Wittinghofer, *J. Biol. Chem.*, 1996, **271**, 6794–6800.
28 H. Kaur, C. S. Park, J. M. Lewis and J. M. Haugh, *Biochem. J.*, 2006, **393**, 235–243.
29 M. E. Pacold, S. Suire, O. Perisic, S. Lara-Gonzalez, C. T. Davis, E. H. Walker, P. T. Hawkins, L. Stephens, J. F. Eccleston and R. L. Williams, *Cell*, 2000, **103**, 931–943.
30 L. Huang, F. Hofer, G. S. Martin and S. H. Kim, *Nat. Struct. Biol.*, 1998, **5**, 422–426.
31 L. Huang, F. Hofer, G. S. Martin and S. H. Kim, *Nat. Struct. Biol.*, 1998, **5**, 422–426.
32 C. P. Ponting and D. R. Benjamin, *Trends Biochem. Sci.*, 1996, **21**, 422–425.
33 C. M. Ragain, R. W. Newberry, A. W. Ritchie and L. J. Webb, *J. Phys. Chem. B*, 2012, **116**, 9326–9336.
34 D. A. Case, T. A. Darden, T. E. Cheatham, C. L. Simmerling, J. Wang, R. E. Duke, R. Luo, R. C. Walker, W. Zhang, K. M. Merz, B. P. Roberts, B. Wang, S. Hayik, A. E. Roitberg, G. Seabra, I. Kolossváry, K. F. Wong, F. Paesani, J. Vanicek, X. Wu, S. R. Brozell, T. Steinbrecher, H. Gohlke, Q. Cai, X. Ye, J. Wang, M. J. Hsieh, G. Cui, D. R. Roe, D. H. Mathews, M. G. Seetin, C. Sagui, V. Babin, T. Luchko, S. Gusarov, A. Kovalenko and P. A. Kollman, *AMBER 11*, University of California, San Francisco, 2010.
35 D. Van der Spoel, E. Lindahl, B. Hess, G. Groenhof, A. E. Mark and H. J. C. Berendsen, *J. Comput. Chem.*, 2005, **26**, 1701–1718.
36 M. W. Mahoney and W. L. Jorgensen, *J. Chem. Phys.*, 2000, **112**, 8910–8922.
37 N. Nassar, G. Horn, C. Herrmann, C. Block, R. Janknecht and A. Wittinghofer, *Nat. Struct. Biol.*, 1996, **3**, 723–729.
38 J. K. Chung, M. C. Thielges, S. R. Lynch and M. D. Fayer, *J. Phys. Chem. B*, 2012, **116**, 11024–11031.
39 A. J. Stafford, D. M. Walker and L. J. Webb, *Biochemistry*, 2012, **51**, 2757–2767.
40 J. R. Reimers and L. E. Hall, *J. Am. Chem. Soc.*, 1999, **121**, 3730–3744.
41 J. H. Choi, K. I. Oh, H. Lee, C. Lee and M. Cho, *J. Chem. Phys.*, 2008, **128**, 134506.
42 D. Dell'Orco, *Mol. BioSyst.*, 2009, **5**, 323–334.

 